

Original Article

De novo cartilage growth after implantation of a 3-D-printed tracheal graft in a porcine model

Sen-Ei Shai^{1,2,3}, Yi-Ling Lai¹, Yi-Wen Hung^{4,5}, Chi-Wei Hsieh⁶, Brian J Huang^{7,8}, Kuo-Chih Su⁹, Chun-Hsiang Wang⁹, Shih-Chieh Hung^{2,7,8}

¹Department of Thoracic Surgery, Taichung Veterans General Hospital, Taiwan; ²Institute of Clinical Medicine, National Yang-Ming University, Taipei, Taiwan; ³National Chi Nan University, Nantou, Taiwan; ⁴Animal Radiation Therapy Research Center, Central Taiwan University of Science and Technology, Taichung, Taiwan; ⁵Terry Fox Cancer Research Laboratory, Translational Medicine Research Center, China Medical University Hospital, Taichung, Taiwan; ⁶Mathematical Gifted Class, Taichung Municipal First Senior High School, Taichung, Taiwan; ⁷Integrative Stem Cell Center, China Medical University Hospital, Taichung, Taiwan; ⁸Institute of New Drug Development, China Medical University, Taichung, Taiwan; ⁹Department of Medical Research, Three Dimensional Printing Research and Development Group, Taichung Veterans General Hospital, Taiwan

Received February 5, 2020; Accepted June 3, 2020; Epub July 15, 2020; Published July 30, 2020

Abstract: Background: Experiments were conducted on the assumption that vivid chondrogenesis would be boosted in vivo following previously preliminary chondrogenesis in a mesenchymal stem cell (MSC)-rich entire umbilical cord (UC) in vitro. Methods: Virtual 3-D tracheal grafts were generated by using a profile obtained by scanning the native trachea of the listed porcine. Although the ultimate goal was the acquisition of a living specimen beyond a 3-week survival period, the empirical results did not meet our criteria until the 10th experiment, ending with the sacrifice of the animal. The categories retrospectively evolved from post-transplant modification due to porcine death using 4 different methods of implantation in chronological order. For each group, we collected details on graft construction, clinical outcomes, and results from both gross and histology examinations. Results: Three animals died due to tracheal complications: one died from graft crush, and two died secondary to erosion of the larger graft into the great vessels. It appeared that the remaining 7 died of tracheal stenosis from granulation tissue. Ectopic de novo growth of neocartilage was found in three porcine subjects. In the nearby tissues, we detected neocartilage near the anastomosis containing interim vesicles of the vascular canals (VCs), perichondrial papillae (PPs) and preresorptive layers (PRLs), which were investigated during the infancy of cartilage development and were first unveiled in the tracheal cartilage. Conclusions: 3-D-printed anatomically precise grafts could not provide successful transplantation with stent-sparing anastomosis; nonetheless, de novo cartilage regeneration in situ appears to be promising for tracheal graft adaptability. Further graft refinement and strategies for managing granulated tissues are still needed to improve graft outcomes.

Keywords: De novo cartilage growth, 3-D-printed tracheal grafts, chondrogenesis

Introduction

Currently, no definitive treatments are available in the event of extensive tracheal resection for either malignant or benign long-segment stenosis. Informative experiments based upon trial-and-error have been cumulative with sporadic success regarding tracheal transplantation using different materials and methods, such as allografts, autografts, prosthetics, autologous tissue-engineered trachea, nanocomposites of tracheal biomaterial with

stem cell seeding, and decellularizing donor trachea [1-8]. The trachea is considered a type of “complex tissue”; therefore, tracheal transplantation should not be equated with transplantation of other organs (i.e., the heart, lung, liver, and kidney) with donor predominance when used in combination with a rejection and anti-rejection regimen dilemma [9].

De novo generation of cartilage within cryopreserved stented aortic allografts has been recently reported [10]. In 2017, Gabner et al.

Neocartilage adjacent to implanted tracheal graft

discovered vascular canals (VCs) in the nose and rib cartilage of newborn piglets to clarify this phenomenon. They claimed that perichondrial papillae (PPs), preresorptive layers (PRLs) and VCs are the major roles for cartilage maturation through cartilage corrosion and the removal of degradation products. The VCs in piglet cartilage provide metabolism for the modulation of the outnumbered chondrocytes in the center of the cartilage and thus remove matrix degradation products [11].

Advanced three-dimensional (3-D) printing technology, a recipient predominant capability, has offered a promising solution towards customizing engineered objects with a shape compatible with a functional trachea for clinical application [12, 13]. The mainstream hypothesis is that this process promotes progenitor or stem cell homing, leading to the de novo generation of cartilage. In this scenario, the organisms are considered to be natural bioreactors and facilitate in vivo airway tissue engineering [14, 15].

Materials and methods

Graft design and components

We harvested fresh native listed porcine tracheae from pigs (~100 kg, 6.5 months old) and stored them in normal saline at 4°C for <24 hours ([Supplementary Figure 1A](#)). A 3-D probe was used to scan the native porcine trachea, with the image results saved in stereolithographic format (STL) (Road Ahead Technologies Consultant Corporation). These grafts with a solid nature were then printed with VisiJet® Crystal Plastic Material using a 3-D project MJP 3600 printer. The printing, which was fabricated in Solidworks software from the scanned files, required 8.9 hours to complete ([Supplementary Figure 1B](#)). Grafts of a variety of sizes, as well as optional suture holes at both ends, were produced. The porcine trachea is shaped like a circle, while the human trachea has a C-shaped predominance; a 3-month-old porcine trachea lumen, which resembles the adult human trachea, cannot be virtually scanned by a probe due to its thinner wall. We used the listed porcine trachea as a model and produced a proportional serially downsized model to match a 3-month-old trachea with 4 available options [including identical (I), larger (L) and smaller (S) sizes] for

practical transplantation through the use of existing software parameters each time. An S2 graft amended with evenly spaced holes allowed for outside tissue ingrowth for epithelium covering.

Tracheal transplantation designs

Tracheal grafts of 2 cm in length were produced for transplantation through various modifications of the native porcine trachea as described below (**Figure 1**). Group IA: resection of a 2 cm anterior (A) C-shaped tracheal cartilage only, with the graft sutured end-to-end along the resection margin to form a connection with the proximal and distal parts of the trachea graft wrapped with the entire UC for primitive chondrogenesis in vitro. Group IC: resection of a 2 cm circumferential (C) trachea, with the graft sutured end-to-end in anastomosed connections with the proximal and distal parts of the trachea. Group L: resection of the trachea in the same manner as group IC, followed by telescopic anastomosis using a larger graft placed between the proximal and distal parts of the trachea graft, which was then covered with gelfoam to prevent friction from nearby tissue. Group S1: resection of the trachea in the same manner as Group IC, with a smaller graft telescopically anastomosed with the proximal and distal parts of the trachea. Group S2: resection of the trachea in the same manner as Group IC, with a smaller graft created with evenly spaced holes through the graft itself, including the edge, and then telescopically anastomosed with the proximal and distal parts of the trachea ([Supplementary Figure 2A, 2B](#)).

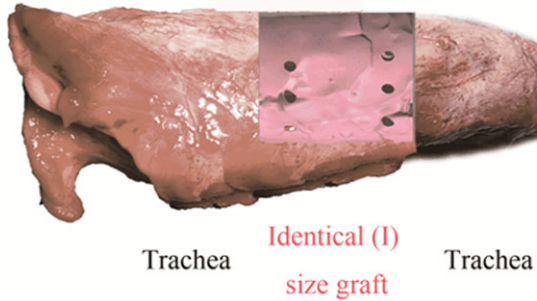
Preparations prior to tracheal transplantation

We used a total of 10 domestic pigs (approximately three months old and weighing between 25 and 40 kg). The experiments were approved by the Institutional Experimentation Committee of Taichung Veterans General Hospital (La-1071538-Animal Welfare Protocol number). Feeding procedures followed both national and international guidelines. Four printed grafts of various sizes, after being refined with polish over the edges and surface, were sterilized using an autoclave after being rinsed with 75% EtOH and 10% H₂O₂ and were

Neocartilage adjacent to implanted tracheal graft

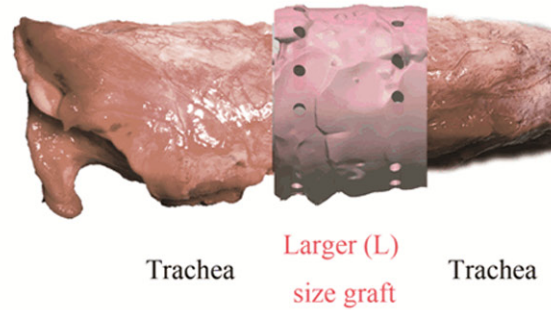
IA (IA-1 to IA-4)

Remove 2 cm C-shape anterior (A)
trachea cartilage only
Proximal/distal anastomosis



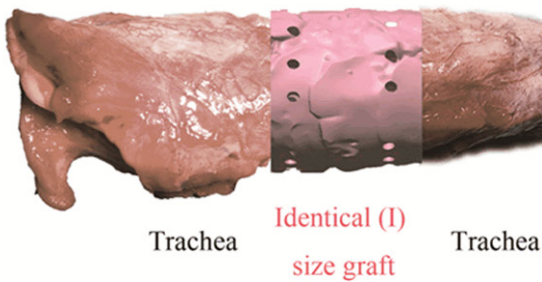
L (L1 and L2)

Remove 2 cm circumferential tracheal ring
Proximal/distal telescoped



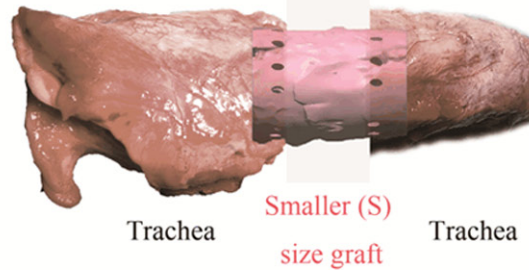
IC (IC-1 and IC-2)

Remove 2 cm circumferential (C) tracheal ring
Proximal/distal anastomosis



S1

Remove 2 cm circumferential tracheal ring
Proximal/distal telescoped



S2

Remove 2 cm circumferential tracheal ring
Proximal/distal telescoped
Scaffold with even distributed holes

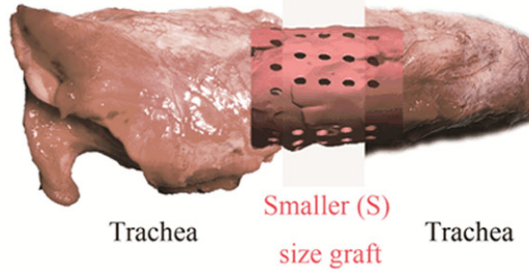


Figure 1. Scheme of the various transplantations of grafts. (IA) Removing the 2 cm C-shape anterior (A) tracheal cartilage only, with the graft end to end anastomosed to the proximal and distal trachea. (IC) Removing the 2 cm circumferential (C) trachea, with the graft end to end anastomosed to the proximal and distal trachea. (L) Removing the 2 cm circumferential trachea, with the proximal/distal trachea telescopically anastomosed with the graft. (S1) Removing the 2 cm circumferential trachea, with the graft telescopically anastomosed to the proximal and distal trachea. (S2) Removing the 2 cm circumferential trachea and the graft with evenly spaced holes telescopically anastomosed to the proximal and distal trachea.

subsequently rinsed with sterile normal saline prior to transplantation.

Surgical transplantation and postoperative care

Surgical procedures were similar in all animal groups (Supplementary Figure 3A-D). Each pig was anesthetized with Zoletil 50 (8 mg/kg, IM,

Virbac, Carros, France), followed by intubation with a 5.5 mm endotracheal tube, and then they were induced under 4 % isoflurane. The animal was placed in a supine position, and the area of skin on the neck was prepared with povidone iodine and 75% alcohol prior to the animal being draped with a disposable sterile towel. After a cervical midline incision and separation of the strap muscles were car-

Neocartilage adjacent to implanted tracheal graft

ried out, adequate exposure of the upper trachea was achieved. A 2 cm long tracheal segment was surgically removed and reconstructed with the 3-D printed tracheal graft ([Supplementary Figure 2](#)). Cross-table ventilation was applied during the creation of the proximal anastomosis. Once the proximal (the same anastomosed procedure as the distal part) and lower posterior half of the distal anastomosis were completed with 4-0 prolene for a continuous running suture, the endotracheal tube was readvanced through the tracheal graft into the distal trachea. The distal anastomosis for the anterior half of the trachea was then completed with interrupted sutures above the endotracheal tube. Last, a tracheal traction suture at the proximal and distal ends was tied together for tension relief over the anastomosis. An airtight seal was confirmed before closing the strap muscles. A silicone Penrose drain was placed, and the wound was closed in layers. Animals were then extubated in the operating room, with all animals recovering uneventfully and resuming both normal activities and oral intake within 12 hours. Postoperative pain relief medication (diclofenac potassium, 25 mg), an antibiotic (ampicillin, 500 mg) and a mucolytic solution (bromhexine hydrochloride, 2 mg/ml) were administered by mixing with food. All animals were managed and administered by the veterinary team.

Gross and histological analyses

Upon animal death or sacrifice, an autopsy was performed, with tissue samples grossly examined prior to being fixed in 10% formalin and embedded with paraffin. Histological staining for glycosaminoglycans (GAGs) was performed using H&E, alcian blue (ScyTek, ANC250) and safranin O/fast green (Cat. #8348a/Cat. #8348b). For chondrocyte markers of collagen II, the proliferating cell nuclear antigen (PCNA) assay detected clearly proliferated cells, while CD31 as a marker of blood vessels in the neocartilage was analyzed with the UltraVision LP Detection System HRP Polymer & DAB Plus Chromogen (Thermo, TL-060-HD). Histological images were obtained on H&E-stained samples, with the images adjusted for optimal brightness using gamma correction. The number of chondrocytes from the raw data was quantified by connected pix-

els, with intensity values exceeding the threshold as calculated by Otsu's method [16]. The summed pixel area within an H&E-stained cartilage section was calculated by its distinct lacuna morphology. We compared the results of the listed mature porcine trachea and the experimental (3-month-old porcine) developing trachea (native & neocartilage).

Statistics

Data (mean \pm SD) were analyzed statistically with the Kruskal Wallis/ANOVA test. A Dunn-Bonferroni test/Bonferroni test was used to compare the numbers of chondrocytes in the cartilage across different tissues. Values of $P < 0.05$ were considered statistically significant.

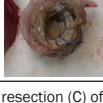
Results

Outcomes and analyses of different transplantations of grafts

Ten consecutive 3-D-printed tracheal grafts were transplanted in 3-month-old porcine allocated to the 4 different groups. Clinical outcomes and the assessment of transplanted graft examinations are summarized in **Table 1**. The procedures conducted on the first two animals (IA-1 and IA-2) were conducted by covering the porcine umbilical cord (UC) with abundant mesenchymal stem cells (MSCs), following previous research for chondrogenesis in vitro, to promote chondrogenesis outside of the tracheal graft ([Supplementary Figure 3E](#)). The IA-1 animal died from a crushed graft due to its thin wall on day 10 after surgery. The IA-2 animal avoided a similar result, as the graft had a thicker wall (1.5 mm). The hemostatic gelfoam covering of the tracheal graft prevented friction caused by nearby blood vessels in the L2 group animal ([Supplementary Figure 3F](#)). However, the L2 animal still died from bleeding due to erosion of larger graft into great vessel on day 6 after surgery in the same manner as the L1 animal. The pigs' survival times extended from 5 to 19 days after surgery. In addition to the three animals (IA-1, L1 and L2) that had died, the remaining 7 animals suffered from tracheal stenosis with fulminating granulation growing around the proximal and distal ends of the anastomosis and, in turn, developed sputum retention (**Table 1**).

Neocartilage adjacent to implanted tracheal graft

Table 1. Summary of data on the transplantation of various grafts and the pathological outcomes

Groups (N)	Weight (kg)	Post-implant status	Survival (day)	Postoperation complications (*day)	Pathology			Cause of death (Grade of stenosis %)
					Proximal trachea (P)	Graft	Distal trachea (D)	
IA-1	25		10	Dyspnea (2~10) Poor appetite (9~10)	N/A	N/A	N/A	Crushed graft (N/A)
IA-2	25		6	Hind limb weakness (4~6) Wound infection (Autopsy)		N/A		Occlusion of proximal and distal anastomosis (P: 10 %; D: 50 %)
IA-3	28		10	N/A				Occlusion of proximal and distal anastomosis (P: 80 %; D: 80 %)
IA-4	30		19	Dyspnea (9~19) *Collapse (9) Vomiting (11~15)				Occlusion of proximal and distal anastomosis (P: 80 %; D: 80 %)
IC-1	25		7	Dyspnea (6~7) Wound infection (Autopsy)	N/A		N/A	Occlusion of proximal and distal anastomosis (N/A)
IC-2	25		14	Dyspnea (7~14) Vomiting (8) Poor appetite (8~14)	N/A	N/A	N/A	Occlusion of proximal and distal anastomosis (N/A)
L1	39		5	N/A				Bleeding (suspected erosion of the jugular vein) (P: 90 %; D: 80 %)
L2	32		6	Dyspnea (4~6) Poor appetite (5~6)	N/A	N/A	N/A	Bleeding (suspected erosion of the jugular vein) (N/A)
S1	37		10	N/A	N/A			Occlusion of proximal and distal anastomosis (P: 90 %; D: 70 %)
S2	37.5		15	Dyspnea (9)				Occlusion of proximal and distal anastomosis (P: N/A; D: 90 %)

Group IA: Resection of anterior (A) C-shaped tracheal cartilage (2 cm) with end-to-end proximal/distal anastomosis. Group IC: Circumferential resection (C) of the trachea (2 cm) with end-to-end proximal/distal anastomosis. Group L: Resection of the whole section of the trachea (2 cm) and scaffold telescope anastomosis into the proximal/distal trachea. Group S1: Resection of the whole section of the trachea (2 cm) and proximal/distal tracheal telescope anastomosis into the scaffold. Group S2: Resection of the whole section of the trachea (2 cm) and proximal/distal trachea telescope anastomosis into the scaffold with evenly distributed holes. P: proximal tracheal stenosis. D: distal tracheal stenosis. *Day after surgery. N/A: none available. *CPR rescue on day 9.

Neocartilage adjacent to implanted tracheal graft

Gross and histological analyses of the grafted samples

Neocartilage growth was detected in tissues outside the tracheal grafts in three of the animals: IA-3, IA-4 and S2. In the S2 animal, an intact layer of tissue formed outside the graft after transplantation ([Supplementary Figure 2C, 2D](#)). Regenerative tissues displayed blood vessels and adipose tissues in the outer layer, along with cartilage containing perichondrium in the middle layer (**Figures 2, 3**). Lucid angiogenesis and condensed immune cells were found in the proximal and distal granulation areas around the tracheal anastomosis (**Figures 2, 3**). In the neocartilage, PPs and VCs, which are regulators of cartilage development, were found at the proximal and distal granulation areas of the tracheal anastomosis (**Figure 3** and [Supplementary Figure 4](#)). The matrix degradation products from chondrocytes (alcian blue and collagen II expression) were detected in the blood vessels of VCs/PPs ([Supplementary Figures 5, 6, 7](#)). Matrix corrosion was indicated by the presence of PRLs and intravascular matrix degradation products [17]. Various stages of developing chondrocytes were found to be distributed in two types of native tracheal cartilage (6.5- and 3-month-old), in neocartilage outside the tracheal graft, and near the anastomosis of the proximal and distal tracheal cartilage tissues (**Figure 4A-J**). The numbers of chondrocytes in the 3-month-old native tracheal cartilage were higher than those in the 6.5-month-old cartilage (171.4 ± 21.1 vs. 65.0 ± 10.2 , respectively, $P < 0.001$). Similar numbers also resulted between those in the neocartilage outside the tracheal graft and those in the 6.5-month-old porcine native trachea (216.1 ± 26.8 vs. 65.0 ± 10.2 , respectively, $P < 0.001$) and those in the 3-month-old porcine native trachea (216.1 ± 26.8 vs. 171.4 ± 21.1 , respectively, $P = 0.082$), along with those in the proximal (216.1 ± 26.8 vs. 106.9 ± 13.1 , respectively, $P < 0.001$) and distal tracheal cartilage (216.1 ± 26.8 vs. 155.0 ± 60.5 , respectively, $P < 0.005$) (**Figure 4K-N**). Safranin O, alcian blue and collagen II as markers of mature chondrocytes were stained positively in the cartilage of native trachea (3-month-old), the neocartilage outside the graft tissue, and the proximal/distal tracheal cartilage (**Figure 5**). All cartilage tissues were stained positively with

alcian blue and collagen II, with the exception of safranin O. The PCNA assay detected clearly proliferated cells in the neocartilage outside the grafts, along with anastomosis near the proximal and distal tracheal cartilage, particularly at the tip of the cartilage (**Figure 6**). In essence, different stages of chondrogenesis were observed in the developing cartilage. At the same time, more blood vessels (in terms of CD31 expression) were formed within the perichondrium of neocartilage outside the tracheal graft and in the nearby proximal/distal tracheal cartilage compared with those in the native tracheal cartilage ([Supplementary Figure 8](#)).

Discussion

Although our ultimate goal was the acquisition of a living specimen beyond a 3-week survival period (a span identical to in vitro chondrogenesis for comparison), the empirical results did not meet our criteria until the 10th experiment ended with an animal being sacrificed. We finalized the research, and analysis was then performed by retrospective grouping in chronological order. We discarded the first two the MSC-rich UC wrapped tracheal graft for boosting cartilage growth as our original design in terms of priority regarding graft implant success, with the remaining 8 being performed using a pure 3-D-printed graft for implantation. Unprecedented dramatic growth in cartilage over the tissue outside the grafts, despite eventual failure in terms of clinical tracheal transplantation for application. Assessments of primitive cartilage growth as follows. First, integral cartilage regenerates rapidly and ectopically for approximately one week. Second, outnumbered chondrocytes are modulated for autodigestion by corona-like VCs derived from the perichondrium, while GAG debris from metabolism appears in the adjacent mucosa and submucosa vessels (**Figure 3** and [Supplementary Figures 4, 5, 6](#)). Third, cartilage elongation mimic sprout-like tapered spears appear along with GAG maturation ([Supplementary Figure 9](#)). Moreover, we detected chondrogenesis in its infancy from sprouting neocartilage during the 6 to 19 day after transplantation (animals IA-2, IA-3, IA-4 and S2). Implanting tracheal grafts may also induce a substantial inflammatory response, causing angiogenesis and adipogenesis with cartilage neoformation at the outside tissues

Neocartilage adjacent to implanted tracheal graft

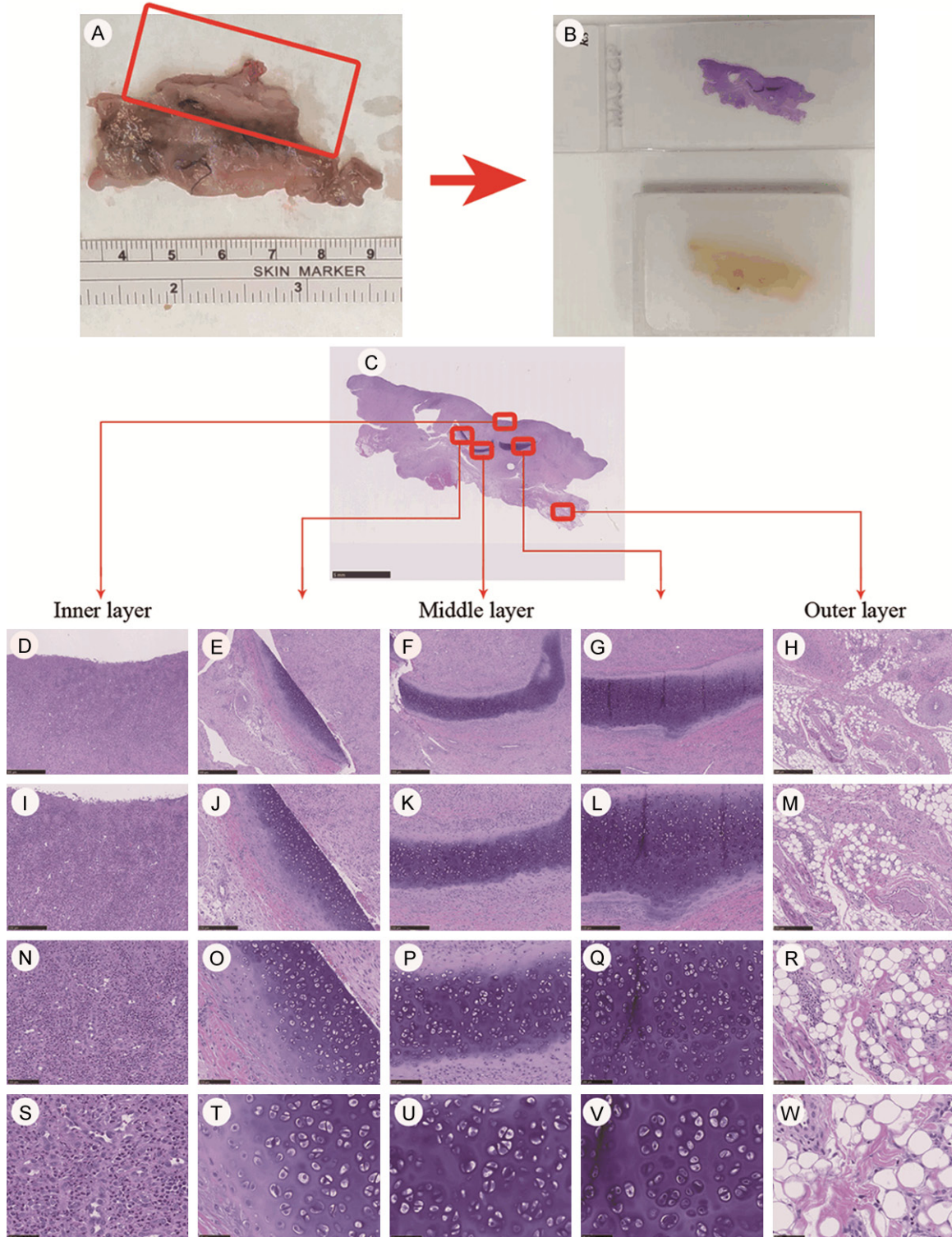
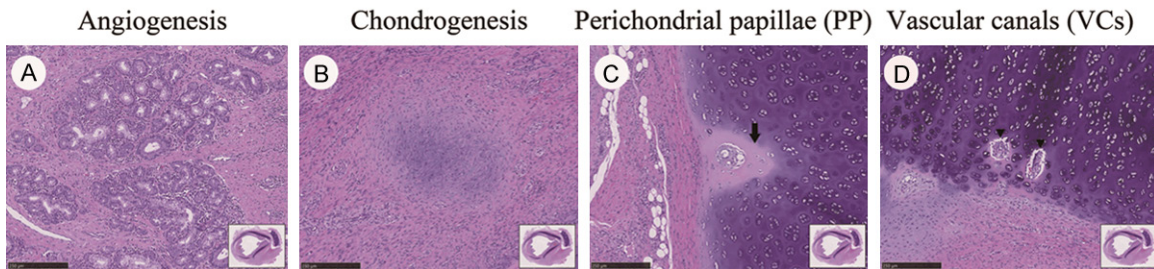


Figure 2. Neof ormation of outside tissues at the tracheal graft (three discrete band-like cartilages with a maximum dimension of 3.78×0.79 mm) (A, B), and results of histological staining (C-W). (A) Specimen from the outside tissue of the tracheal graft. (B) H&E stained and paraffin-embedded outside tissue of the tracheal graft. (C) Full view of H&E stain in the outside tissue of the tracheal graft. (D, I, N, S) Immune cells condensing in the inner layer of the outside tissue of the tracheal graft. (E-G, J-L, O-Q, S-V) Neocartilage forming in the middle layer of the outside tissue of the tracheal graft. (H, M, R, W) Adipose tissue forming in the outer layer of the outside tissue of the tracheal graft. Magnification: 50×/100×/200×/400×, from top to bottom.

Neocartilage adjacent to implanted tracheal graft

Proximal granulation area of tracheal anastomosis



Distal granulation area of tracheal anastomosis

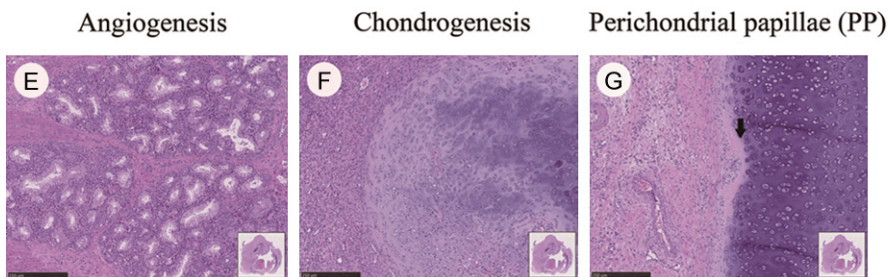


Figure 3. Histological staining in the proximal (A-D) and distal (E-G) granulation area of tracheal anastomosis. (A, E) Intense angiogenesis in the proximal and distal granulation area of the tracheal graft anastomosis. (B, F) Marked chondrogenesis in the proximal and distal granulation areas of tracheal graft anastomosis. (C, G) The formation of perichondrial papillae (PP) from the perichondrium in the proximal and distal granulation areas of tracheal anastomosis. PP, showing perpendicular growth out of the perichondrium, protruding inward to the cartilage matrix. Black arrow: preresorptive layers (PRLs). (D) The independent vascular canals (VCs) in the proximal granulation area of tracheal anastomosis. VCs, migrated from the perichondrium and lingering around the overpopulous infant chondrocytes. Magnification $\times 100$, H&E stain.

(**Figure 2**). Chondrogenesis, angiogenesis, and adipogenesis indicated with MSC migration to the graft area for the regeneration [18]. In vivo, MSCs sourcing from blood and adipose tissue induce chondrogenesis through stimulation with endogenous TGF- β mostly from chondrocytes [19].

Chondrogenesis in the proximal/distal granulation area of the tracheal anastomosis revealed that PPs, PRLs and VCs all participated in cartilage development through the processes of corrosion and matrix degradation by way of chondrolysis in order to reach homeostasis (animal S2) (**Figure 3**). Besides, we detected matrix degradation products (alcian blue and collagen II expression) within the blood vessels of VCs/PPs (**Figure 3** and [Supplementary Figures 4, 5, 6](#)). Additional degradation debris was found in both the vessels and on the surface of the granulation tissue of the proximal and distal trachea, particularly the proximal trachea ([Supplementary Figure 6](#)). Degraded matrix material can be dif-

fusely distributed in the canal's stroma next to the PRL, within capillaries and in the associated downstream veins of the VCs, along with the veins outside the perichondrium at some distance from the cartilage surface. These phenomena reflect the underlying processes of vascular transport and removal [17].

The density and distribution of chondrocytes were different in the porcine native tracheae (6.5-month-old and 3-month-old), neocartilage outside the tracheal graft, and the proximal/distal tracheal graft end neocartilage. According to histological analysis, more oval-shaped and larger cells were found in the 6.5-month-old native porcine tracheal cartilage than in its 3-month-old counterpart. H&E, safranin O, alcian blue and collagen II staining appeared similar in the porcine native tracheal cartilage (3-month-old) (**Figure 5A-D**). Safranin O staining was particularly weak in both the posterior tracheal cartilage and tracheal islands (**Figure 5B**). We recognized the neocartilage through the low levels of H&E, safranin O, alcian

Neocartilage adjacent to implanted tracheal graft

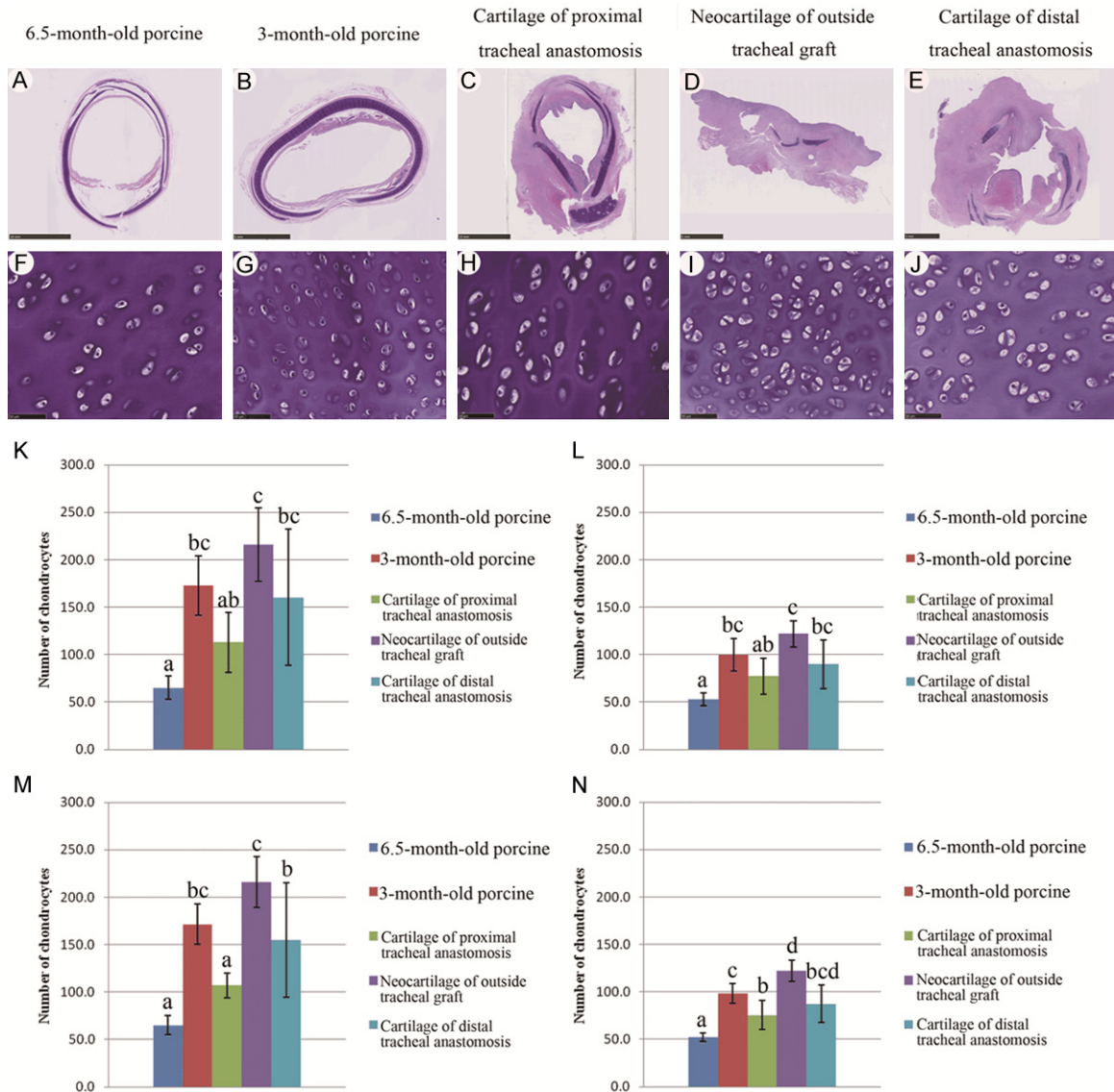


Figure 4. Morphology and number of chondrocytes compared between the two ages of animals (6.5- and 3-month-old porcine native trachea, proximal/distal tracheal cartilage, and tracheal graft neocartilage). A-E. Full view of H&E staining in the two ages (6.5- and 3-month-old) porcine native trachea, proximal/distal tracheal cartilage, and tracheal graft neocartilage. F-J. Morphology and density of chondrocytes in histological staining. Magnification 400 \times . K, M. Randomly captured images and the number of chondrocytes quantified according to the Otsu method. L, N. Randomly captured images and the number of chondrocytes quantified by the artificial method. K, L. Total numbers of chondrocytes (N = 10 in each group) were calculated. M, N. Total numbers of chondrocytes (N = 8 in each group) were calculated after deleting outliers. a, b, c, d: showing significant differences across groups (P < 0.05).

blue and collagen II staining (Figure 5). The matrix was formed in a weak manner even in mature chondrocytes (clear lacuna, clusters of chondrocytes) (Figure 5M-P). Chondroblasts and chondroprogenitor cells with proliferation potential were found near the edge of both the 6.5-month-old and 3-month-old tracheal cartilage and neocartilage in the outside tracheal grafts (Supplementary Figure 10).

Cartilage islands and templates were also detected in the same area (Supplementary Figure 11).

We detected PCNA expression and found lower expression of the proliferation marker PCNA in the 3-month-old native trachea (Figure 6A-C), which further showed that these proliferating cells could reach a mature stage towards

Neocartilage adjacent to implanted tracheal graft

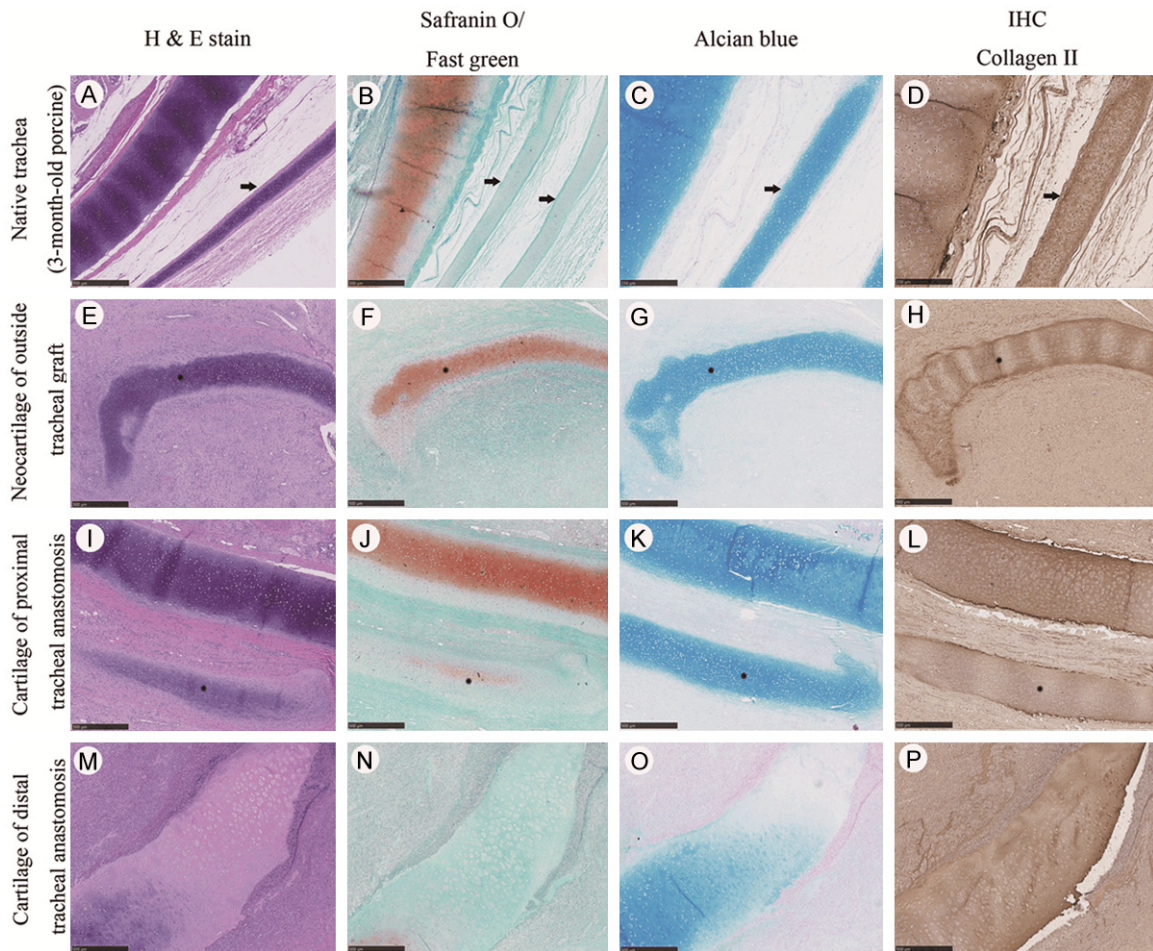


Figure 5. Various stainings in porcine native trachea, the outside tissues of the graft, and the proximal and distal trachea. A-D. Strong staining to H&E, alcian blue and collagen II, and weak staining to safranin O in cartilage templates of native trachea. Black arrow: cartilage templates. E-L. Strong staining to H&E, alcian blue and collagen II, and weak staining to safranin O in neocartilages of the outside tissues of the graft and proximal trachea. Black star: neocartilage. M-P. Weak or no staining in clusters of chondrocytes with clear lacuna. Magnification 50 \times .

stable chondrocytes by fading the marker. At the same time, at the edge of the neocartilage in the proximal/distal trachea (**Figure 6I** and **6L**), and in the outside tissues of the tracheal grafts (**Figure 6D-H**, **6J** and **6K**), we detected PCNA-positive cells with a proliferation potential greater in number than what was found only in the native tracheal cartilage itself. Furthermore, a more well-defined and well-distinguished perichondrium appeared in the cartilage of the native trachea than it did in either the new cartilage near the proximal trachea, outside the tracheal grafts or around the distal trachea. Additionally, we also found chondroblasts extending from some areas of the neocartilage (**Supplementary Figure 9**).

Interestingly, the safranin O, alcian blue and collagen II stains not only distinguished neocartilage but also differentiated VCs that did not show staining for safranin O and only showed weak staining for alcian blue and collagen II (**Supplementary Figures 4, 5**). More degradation products (alcian blue expression) were found in both the blood vessels and on the surface of the granulation tissue of the proximal and distal trachea, particularly in the overgrowing granulation tissues of the proximal trachea. These staining patterns appeared to positively correlate with the number of VCs (**Supplementary Figure 6**). VCs/PPs were found not only in the cartilage of the near proximal and distal trachea but also in the 3-month-old

Neocartilage adjacent to implanted tracheal graft

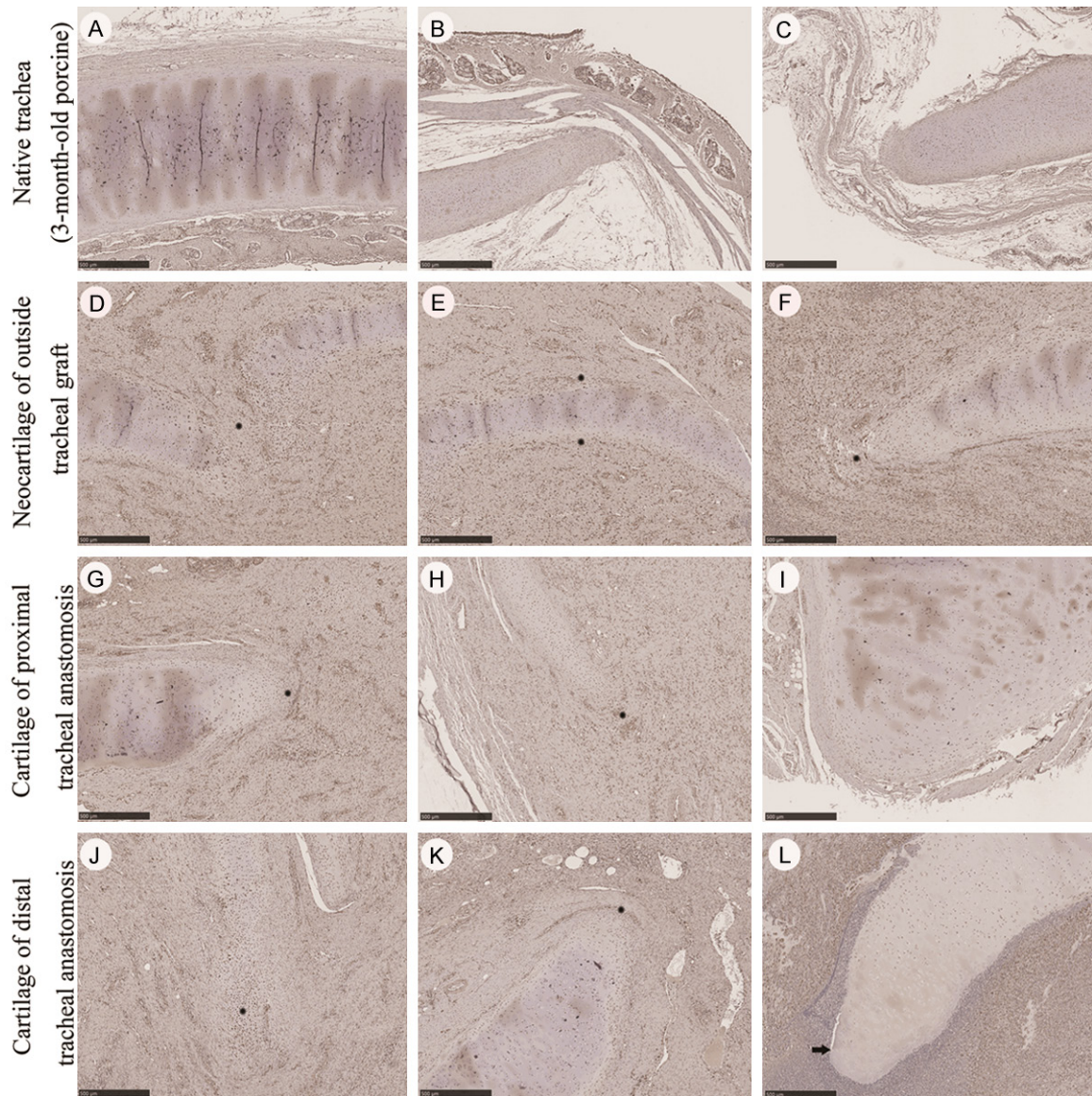


Figure 6. Immunohistochemistry stainings for proliferating cell nuclear antigen (PCNA) in porcine native trachea, the outside tissues of graft, proximal and distal tracheae. A-C, I. Scarcity of PCNA-positive cells in the native trachea and proximal trachea. D-H, J, K. More PCNA-positive cells in the neocartilage of the outside tissues of graft, proximal and distal tracheae. Black star: PCNA-positive cell in the neocartilage. L. An absence of PCNA-positive cells in the distal trachea. Black arrow: absence of PCNA-positive cells. Magnification 50 \times .

native tracheal cartilage. However, we found no VCs/PPs in the 6.5-month-old native tracheal cartilage. These VCs/PPs might only be found in areas of dense chondrocytes. The cell densities and clusters of neocartilage were more abundant at the outside tracheal grafts (Figure 4), with a greater expression of the proliferated marker PCNA than in the native tracheal cartilage (Figure 6).

In conclusion, 3-D-printed tracheal grafts could readily provide de novo cartilage growth with stent-sparing anastomosis, although they could

not provide successful transplantation in a porcine model. Cartilage regeneration in situ has enlightened us towards implementing advanced 3-D printing technology with customized tissues and size-matched counterparts. This appears to be a promising and viable option for tracheal graft adaptability.

Acknowledgements

The authors sincerely appreciate the assistance of the Center for Translational Medicine, Department of Medical Research 3D Printing

Neocartilage adjacent to implanted tracheal graft

Research and Development Group, Biostatistics Task Force and Center of Quantitative Imaging in Medicine, Department of Medical Research, Taichung Veterans General Hospital, Taichung, Taiwan.

Disclosure of conflict of interest

None.

Address correspondence to: Dr. Shih-Chieh Hung, Institute of New Drug Development, China Medical University, Taichung, Taiwan; Integrative Stem Cell Center, China Medical University Hospital, Taichung Joint PI, IBMS, Academia Sinica 7F, No. 6, Xueshi Rd., North Dist., Taichung City 404, Taiwan. Tel: +886-4-2205-2121 Ext. # 7728, +886-952-53-2728; E-mail: hung3340@gmail.com

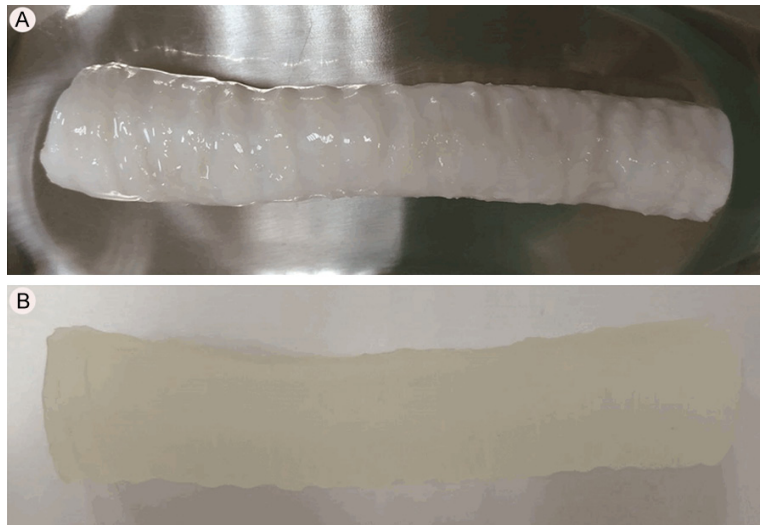
References

- [1] Lano CF Jr, Duncavage JA, Reinisch L, Ossoff RH, Courey MS and Netterville JL. Laryngo-tracheal reconstruction in the adult: a ten year experience. *Ann Otol Rhinol Laryngol* 1998; 107: 92-7.
- [2] Tan A, Cheng S, Cui P, Gao P, Luo J, Fang C and Zhao Z. Experimental study on an airway prosthesis made of a new metastable β -type titanium alloy. *J Thorac Cardiovasc Surg* 2011; 141: 888-894.
- [3] Kojima K, Bonassar LJ, Roy AK, Vacanti CA and Cortiella J. Autologous tissue-engineered trachea with sheep nasal chondrocytes. *J Thorac Cardiovasc Surg* 2002; 123: 1177-1184.
- [4] Tsukada H, Gangadharan S, Garland R, Herth F, DeCamp M and Ernst A. Tracheal replacement with a bioabsorbable scaffold in sheep. *Ann Thorac Surg* 2010; 90: 1793-1797.
- [5] Shin YS, Choi JW, Park JK, Kim YS, Yang SS, Min BH and Kim CH. Tissue-engineered tracheal reconstruction using mesenchymal stem cells seeded on a porcine cartilage powder scaffold. *Ann Biomed Eng* 2015; 43: 1003-13.
- [6] Kim DY, Pyun J, Choi JW, Kim JH, Lee JS, Shin HA, Kim HJ, Lee HN, Min BH, Cha HE and Kim CH. Tissue-engineered allograft tracheal cartilage using fibrin/hyaluronan composite gel and its in vivo implantation. *Laryngoscope* 2010; 120: 30-38.
- [7] Kamil SH, Eavey RD, Vacanti MP, Vacanti CA and Hartnick CJ. Tissue-engineered cartilage as a graft source for laryngotracheal reconstruction: a pig model. *Arch Otolaryngol Head Neck Surg* 2004; 130: 1048-51.
- [8] Tsukada H, Gangadharan S, Garland R, Herth F, DeCamp M and Ernst A. Tracheal replacement with a bioabsorbable scaffold in sheep. *Ann Thorac Surg* 2010; 90: 1793-7.
- [9] Claesson-Welsh L and Hansson GK. Tracheo-bronchial transplantation: the royal swedish academy of sciences' concerns. *Lancet* 2016; 387: 942.
- [10] Zang M, Zhang Q, Davis G, Huang G, Jaffari M, Ríos CN, Gupta V, Yu P and Mathur AB. Perichondrium directed cartilage formation in silk fibroin and chitosan blend scaffolds for tracheal transplantation. *Acta Biomater* 2011; 7: 3422-31.
- [11] Gabner S, Häusler G and Böck P. Vascular canals in permanent hyaline cartilage: development, corrosion of nonmineralized cartilage matrix, and removal of matrix degradation products. *Anat Rec (Hoboken)* 2017; 300: 1067-1082.
- [12] Bhora FY, Lewis EE, Rehmani SS, Ayub A, Raad W, Al-Ayoubi AM and Lebovics RS. Circumferential three-dimensional-printed tracheal grafts: research model feasibility and early results. *Ann Thorac Surg* 2017; 104: 958-963.
- [13] Rehmani SS, Al-Ayoubi AM, Ayub A, Barsky M, Lewis E, Flores R, Lebovics R and Bhora FY. Three-dimensional-printed bioengineered tracheal grafts: preclinical results and potential for human use. *Ann Thorac Surg* 2017; 104: 998-1004.
- [14] Martinod E, Chouahnia K, Radu DM, Joudiou P, Uzunhan Y, Bensidhoum M, Santos Portela AM, Guiraudet P, Peretti M, Destable MD, Solis A, Benachi S, Fialaire-Legendre A, Rouard H, Collon T, Piquet J, Leroy S, Vénissac N, Santini J, Tresallet C, Dutau H, Sebbane G, Cohen Y, Beloucif S, d'Audiffret AC, Petite H, Valeyre D, Carpentier A and Vicaut E. Feasibility of bioengineered tracheal and bronchial reconstruction using stented aortic matrices. *JAMA* 2018; 319: 2212-2222.
- [15] Martinod E, Paquet J, Dutau H, Radu DM, Bensidhoum M, Abad S, Uzunhan Y, Vicaut E and Petite H. In vivo tissue engineering of human airways. *Ann Thorac Surg* 2017; 103: 1631-1640.
- [16] Jungebluth P, Go T, Asnaghi A, Bellini S, Martorell J, Calore C, Urbani L, Ostertag H, Mantero S, Conconi MT and Macchiarini P. Structural and morphologic evaluation of a novel detergent-enzymatic tissue-engineered tracheal tubular matrix. *J Thorac Cardiovasc Surg* 2009; 138: 586-93.
- [17] Ponte AL, Marais E, Gallay N, Langonné A, Delorme B, Hérault O, Charbord P and Domenech J. The in vitro migration capacity of human bone marrow mesenchymal stem cells:

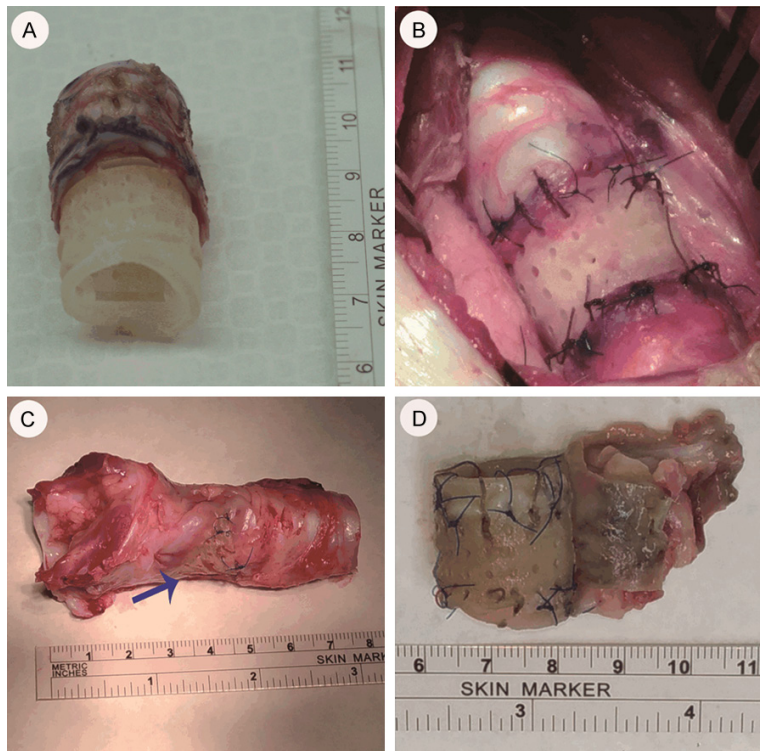
Neocartilage adjacent to implanted tracheal graft

- comparison of chemokine and growth factor chemotactic activities. *Stem Cells* 2007; 25: 1737-1745.
- [18] Baumann K. Stem cells: moving out of the niche. *Nat Rev Mol Cell Biol* 2014; 15: 79.
- [19] Chen MJ, Whiteley JP, Please CP, Ehlicke F, Waters SL and Byrne HM. Identifying chondrogenesis strategies for tissue engineering of articular cartilage. *J Tissue Eng* 2019; 10: 2041731419842431.

Neocartilage adjacent to implanted tracheal graft

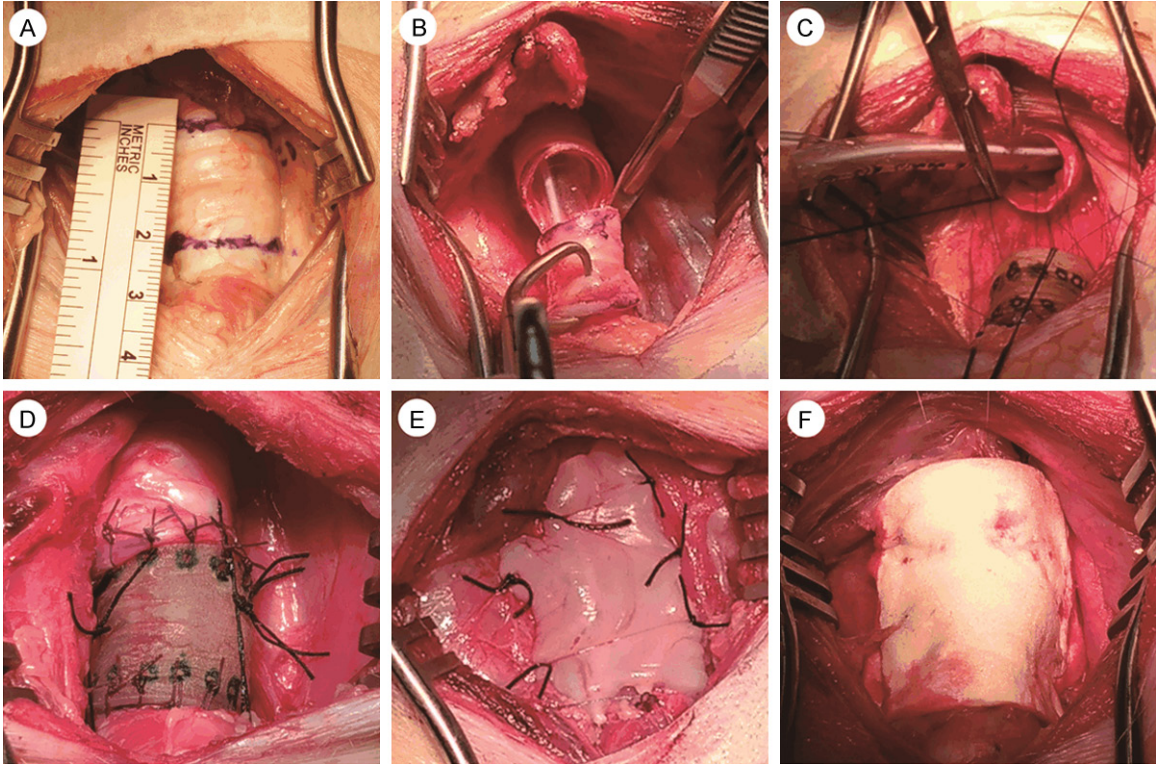


Supplementary Figure 1. Native tracheal tissue of listed porcine. A. A long segment of fresh native listed porcine trachea acquired and immersed in 0.9% normal saline >24 hours at 4 °C (an approximately 100 kg, 6.5-month-old pig). B. 3-D printed using a crystal ingredient with an imitation of the fresh native listed porcine trachea as computer-scanned. Tracheal size: 120×25×3 mm.



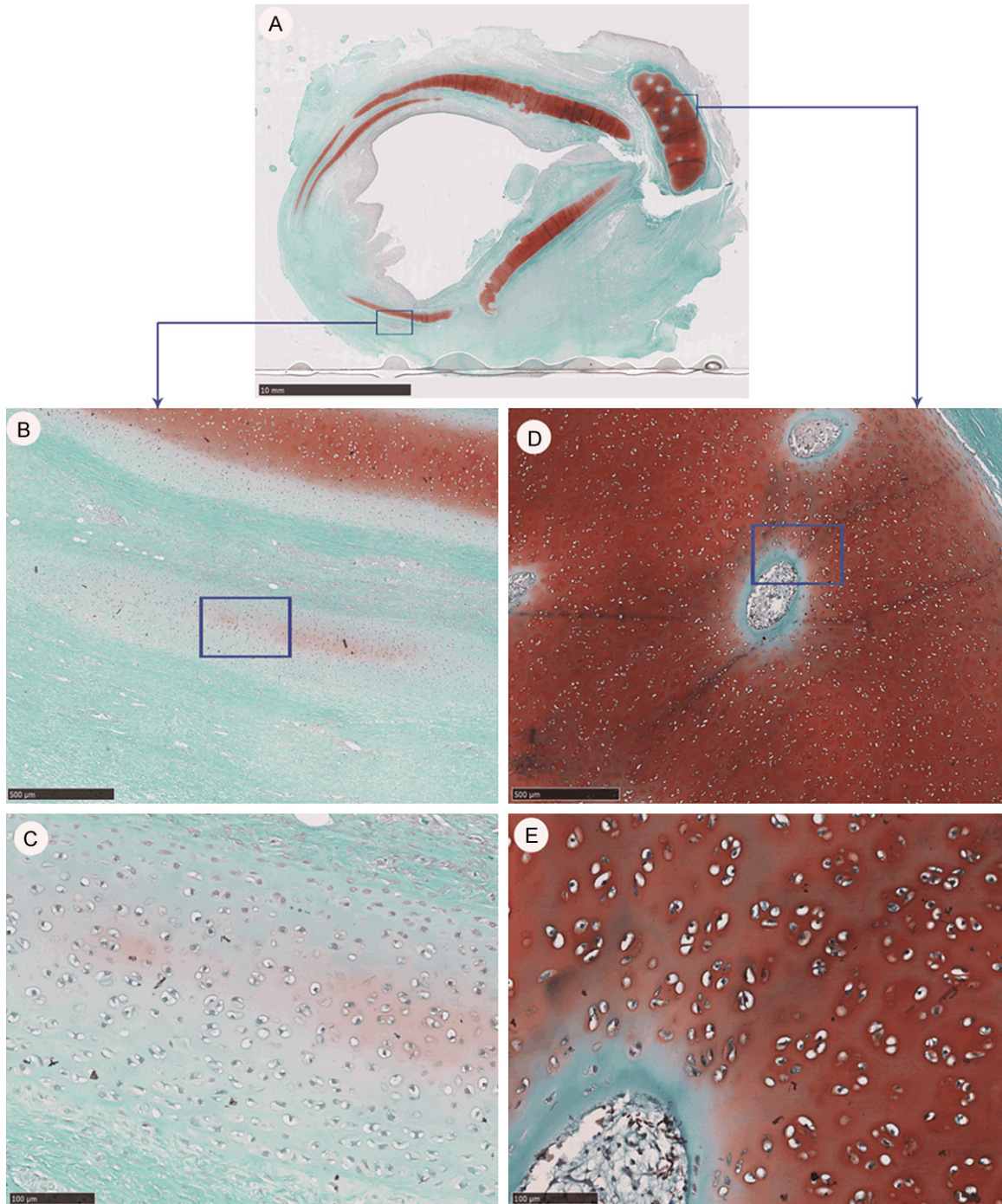
Supplementary Figure 2. Tracheal graft implantation in animal S2 and its autopsy picture afterwards. A. Resected porcine trachea fitted to the tracheal graft prior to implantation in Group S. B. Finalizing implantation of the graft with evenly-spaced holes under a telescopic view. Red arrow: tracheal graft. C. External view of the porcine tracheal tissue. D. Integrated tissue covering the graft with easy detachment. Unfolding tissue outside the tracheal graft.

Neocartilage adjacent to implanted tracheal graft



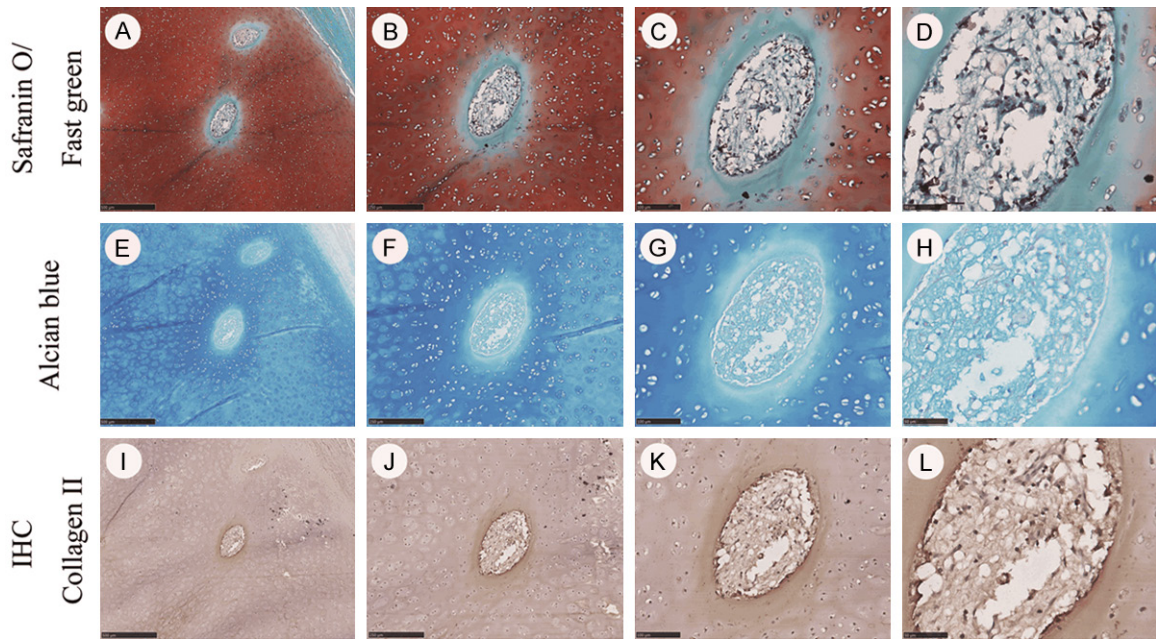
Supplementary Figure 3. Surgical procedure for tracheal graft transplantation. A. Marking a 2 cm-long region on the trachea. B. Cutting the marked distal trachea. C. Anastomosis of the proximal trachea was performed using 4-0 sutures. D. The anastomosis to the proximal and distal tracheae after graft transplantation. E. Covering the porcine umbilical cord (UC) after graft transplantation to induce mesenchymal stem cells (MSCs) for UC migration. F. Covering with hemostatic gel foam to minimize friction between the bulging tracheal graft and internal carotid artery in the L group.

Neocartilage adjacent to implanted tracheal graft



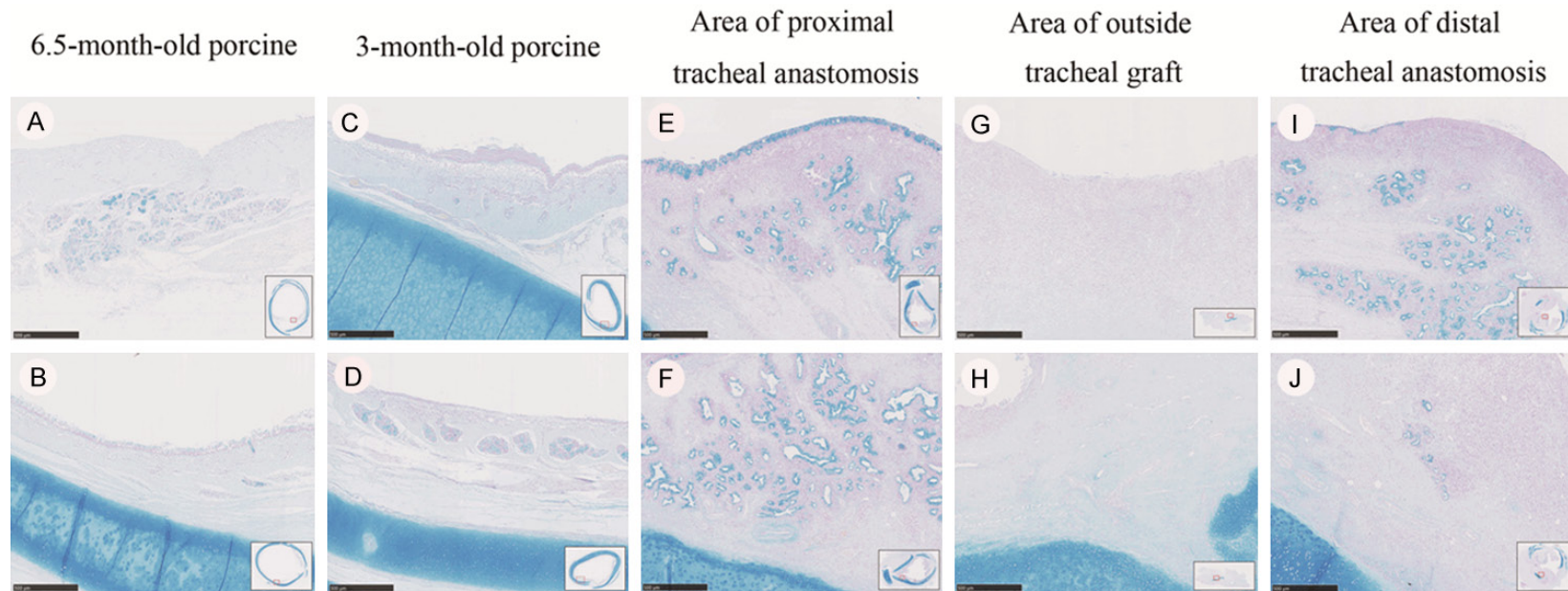
Supplementary Figure 4. Safranin O/fast green staining in the proximal granulation area of the tracheal anastomosis. (A) Holoscopic view of safranin O/fast green staining in the proximal granulation area of the tracheal anastomosis. (B) Weak safranin O expression in the neocartilage of the proximal granulation area of the tracheal anastomosis $\times 50\times$. (C) Safranin O/fast green staining at high magnification ($200\times$) - same area as the blue box in (B). Note the abundance of chondrocytes with weak staining for glycosaminoglycans (GAGs) and the absence of VCs in this area of neocartilage. (D) Strong safranin O expression in the mature cartilage of the proximal granulation area of the tracheal anastomosis $\times 50\times$. (E) Safranin O/fast green staining at high magnification ($200\times$) - same area as the blue box in (D). Note the abundance of chondrocytes with large amounts of GAGs and the presence of multiple VCs in this area of primitive cartilage. Magnification: $100\times/200\times/400\times$, from left to right.

Neocartilage adjacent to implanted tracheal graft



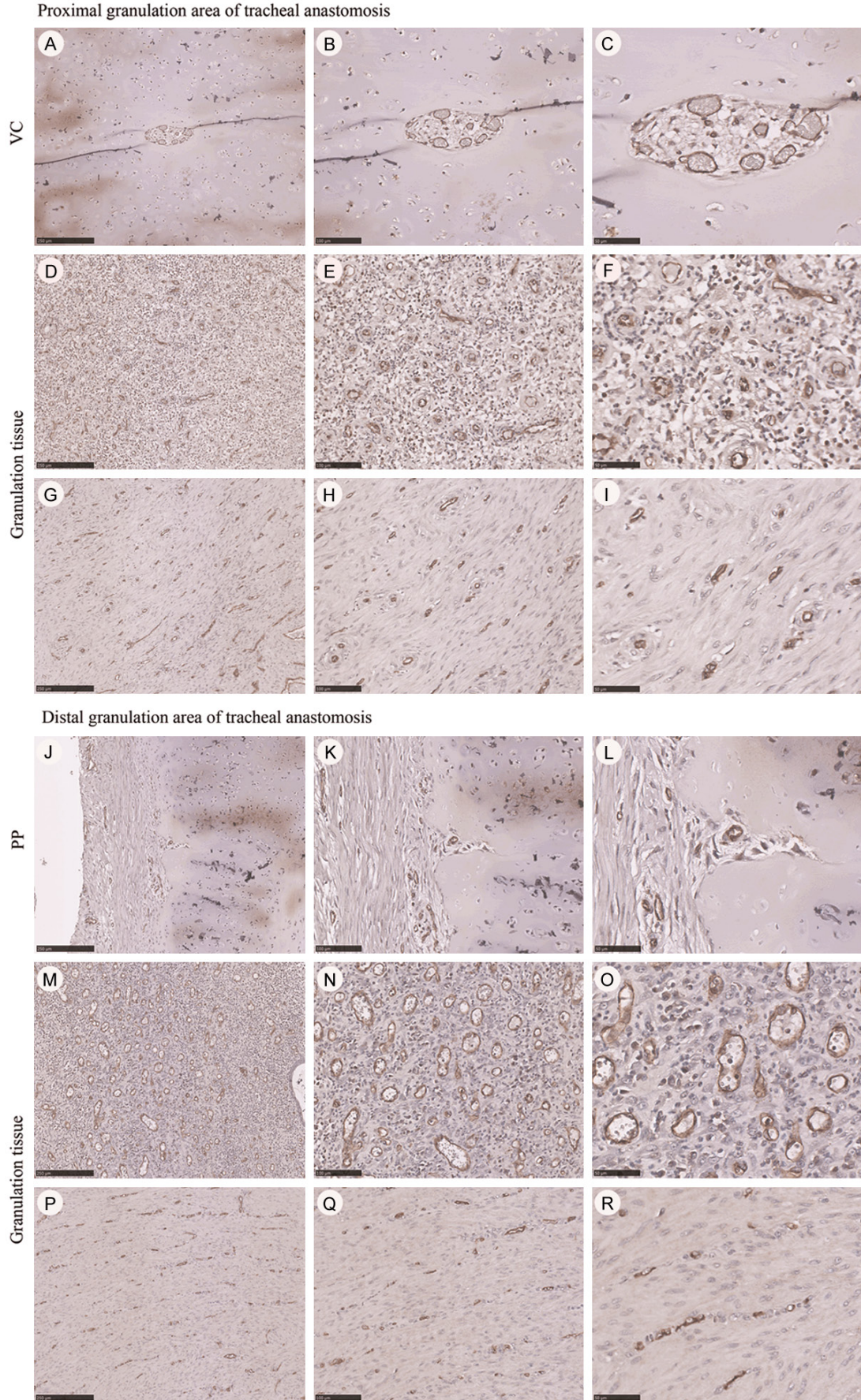
Supplementary Figure 5. Various levels of staining in VCs from proximal tracheal cartilage. A. Two separate migratory VCs that act like icebreakers for the modified mature chondrocytes. B. A ruby-chestnut-colored background filled with GAG matrix distributed with unduly chondrocytes, contrasted with the corona-like elliptical VC-fading radiant blue-tinged ring due to vanishing GAGs. C. A magnified view of a solitary VC $\times 200\times$. D. Views of the inner VC showing capillaries, extravasation of erythrocytes, and fibroblasts $\times 400\times$. A-D. Strong safranin O staining in the cartilage and an abundance of chondrocytes. Note VCs without safranin O staining in the process of lysing the cartilage matrix (green area around VCs). E-H. Matrix (GAG) degradation products detected weakly within the VCs with alcian blue staining. Matrix degradation products can be transported via the blood vessels in VCs. I-L. Fibers of VCs detected weakly with collagen II staining. Magnification: $50\times/100\times/200\times/400\times$, from left to right.

Neocartilage adjacent to implanted tracheal graft



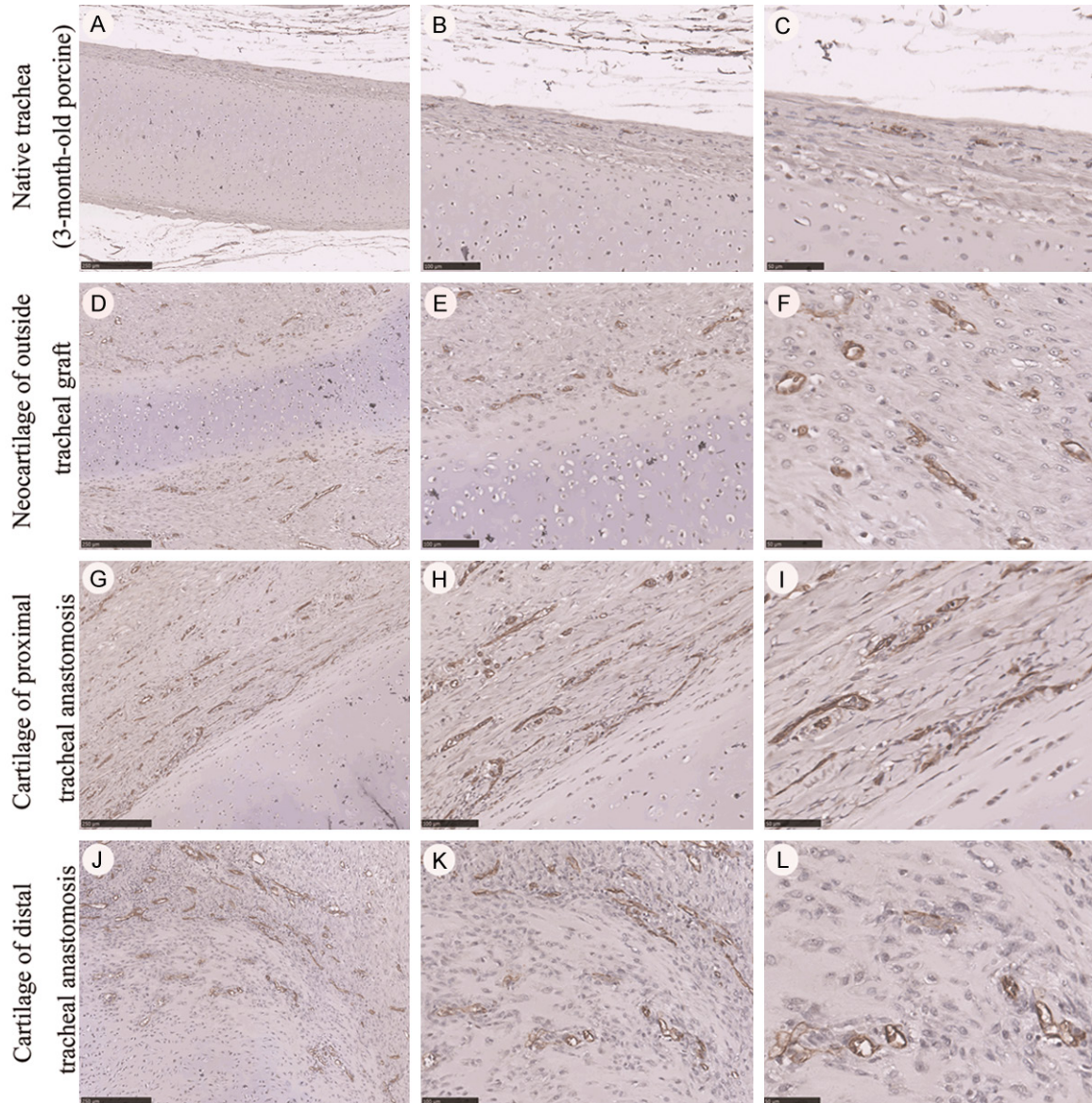
Supplementary Figure 6. Matrix degradation products found within the mucosa and submucosa vessels beneath the cartilage of the native porcine trachea (6.5- and 3-month-old), in the area of the proximal/distal trachea, and in the area outside of the tracheal graft-like sewage work. A. Scarcity of matrix degradation products within vessels near the surface of the 6.5-month-old porcine tracheal epithelium. B. Scarcity of matrix degradation products within vessels around the cartilage of the 6.5-month-old porcine trachea. C. Scarcity of matrix degradation products within vessels near the surface of the 3-month-old porcine tracheal epithelium. D. Scarcity of matrix degradation products within vessels around the cartilage of the 3-month-old porcine trachea. E. Abundance of matrix degradation products within vessels near the surface of the granulation tissue area of the proximal trachea. F. Abundance of matrix degradation products within vessels around the cartilage in the area of the proximal trachea. G. Scarcity of matrix degradation products within vessels near the surface of the outside tissue of the tracheal graft. H. Scarcity of matrix degradation products within vessels around the neocartilage area outside the tracheal tissue graft. I. Abundance of matrix degradation products within vessels near the surface of the granulation tissue area of the distal trachea. J. Abundance of matrix degradation products within vessels around the cartilage area of the distal trachea. Magnification $\times 50\times$.

Neocartilage adjacent to implanted tracheal graft



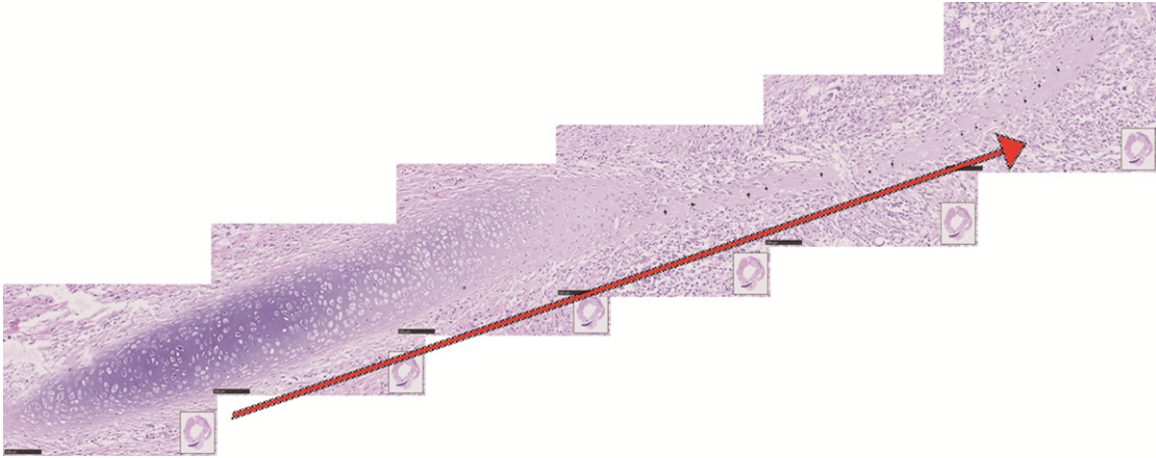
Neocartilage adjacent to implanted tracheal graft

Supplementary Figure 7. CD31 staining by IHC in the proximal (A-I) and distal (J-R) granulation areas of the tracheal anastomosis. (A-C) CD31 expressions of blood vessels in the proximal distal granulation area of tracheal graft anastomosis. (D-I) CD31 expressions of blood vessels in the granulation tissue of proximal area of tracheal graft anastomosis. (J-L) CD31 expressions of blood vessels in the PP of distal distal granulation area of tracheal graft anastomosis. (M-R) CD31 expressions on blood vessels in the granulation tissue of distal area of tracheal graft anastomosis. CD31 expression: brown. Magnification: 100×/200×/400×, from left to right.

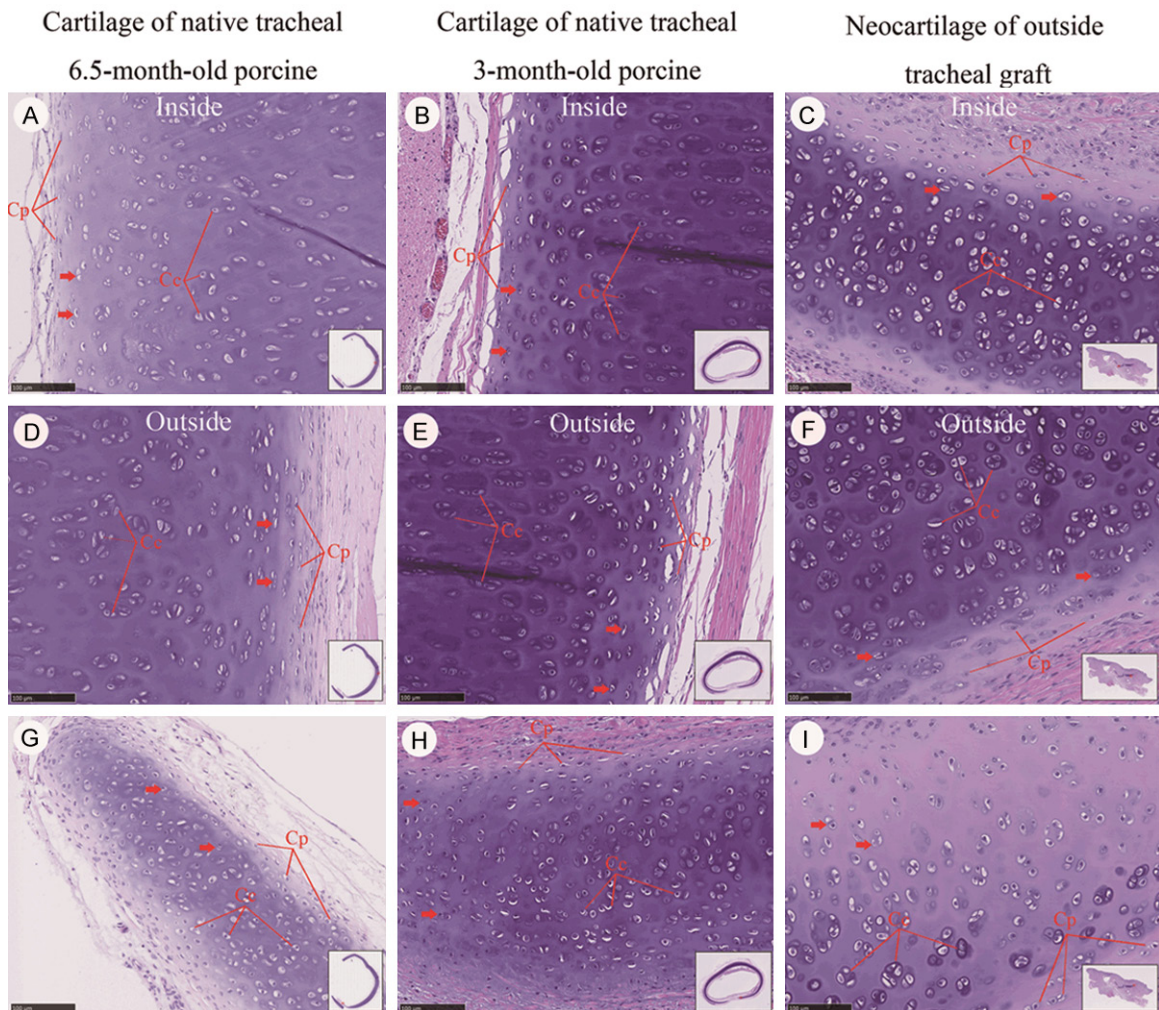


Supplementary Figure 8. CD31 staining by IHC in porcine native trachea, the outside tissue of the graft, proximal and distal tracheae. A-C. Scarcity of blood vessels in the perichondrium of native porcine trachea. D-L. Abundance of blood vessels in the perichondrium neocartilage of the outside tissues of the graft, cartilage of proximal and distal tracheae. CD31 expression: brown. Magnification: 100×/200×/400×, from left to right.

Neocartilage adjacent to implanted tracheal graft

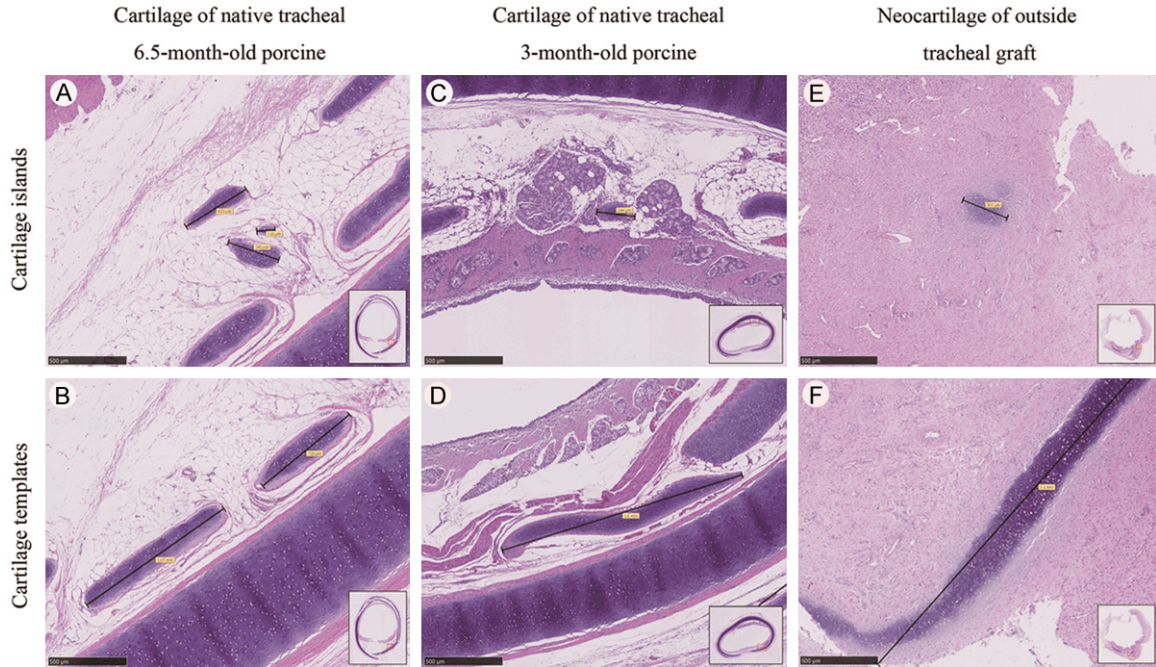


Supplementary Figure 9. Evolution in tapered spear-like neocartilage with elongation in the trachea. De novo cartilage growth after tracheal transplantation in a porcine preparation using a mock-up three-dimensional-printed graft, with access to its tissue regeneration and early structural integrity.



Supplementary Figure 10. Distribution of chondroblasts (Cb), chondrocytes (Cc) and chondroprogenitor cells (Cp) in the 6.5- and 3-month-old native tracheal cartilage or neocartilage tissues outside the tracheal graft. A, D, G. Limited numbers of Cbs, Ccs and Cps in 6.5-month-old native tracheal cartilage. B, E, H. Abundance of Cbs, Ccs and Cps in 3-month-old native tracheal cartilage. C, F, I. Abundance of Cbs, Ccs, Cps and clusters of chondrocytes in the neocartilage of the outside tracheal graft. Red arrows: chondroblasts. Magnification $\times 200\times$, H&E staining.

Neocartilage adjacent to implanted tracheal graft



Supplementary Figure 11. Cartilage islands and templates in native (6.5- and 3-month-old) trachea and neocartilage of the outside tracheal graft. A, B. Cartilage islands and templates with well-distinguished perichondrium in the 6.5-month-old porcine native trachea. C, D. Cartilage islands and templates with well-distinguished perichondrium in 3-month-old porcine native trachea. E, F. Cartilage islands and templates without well-distinguished perichondrium in the neocartilage of the outside tracheal graft. Magnification $\times 50\times$.